

# The Baryonic Halos of Elliptical Galaxies: Radial Distribution of Globular Clusters and Diffuse Hot Gas

Duncan A. Forbes<sup>1\*</sup>, Trevor Ponman<sup>2</sup> and Ewan O’Sullivan<sup>2,3</sup>,

<sup>1</sup>*Centre for Astrophysics & Supercomputing, Swinburne University, Hawthorn VIC 3122, Australia*

<sup>2</sup>*School of Physics and Astronomy, University of Birmingham, Edgbaston, Birmingham B15 2TT*

<sup>3</sup>*Harvard-Smithsonian Center for Astrophysics, 60 Garden Street, Cambridge, MA 02138, USA*

13 September 2018

## ABSTRACT

For a sample of 9 well-studied giant ellipticals we compare the projected radial distribution of their red and blue globular cluster (GC) subpopulations with their host galaxy stellar and X-ray surface brightness profiles. We support previous findings that the surface density distribution of *red* (metal-rich) GCs follows that of the host galaxy starlight. We find good agreement between the outer slope of the *blue* GC surface density and that of the galaxy X-ray emission. This coincidence of projected radial profiles is likely due to the fact that both blue GCs and X-ray emitting hot gas share the same gravitational potential in equilibrium. When deprojected the X-ray emitting hot gas has a radial density dependence that is the square root of that for the GC density. We further show that the energy per unit mass for blue GCs is roughly half that of the hot gas.

**Key words:** globular clusters: general – galaxies: star clusters – galaxies: individual – galaxies: formation

## 1 INTRODUCTION

The globular cluster (GC) systems of most, well-studied large galaxies reveal evidence for two subpopulations in colour (and by proxy in metallicity). Soon after the discovery of two subpopulations, it was shown that they have different spatial distributions with the *red* (metal-rich) subpopulation being more centrally concentrated than the more extended *blue* (metal-poor) one (see Brodie & Strader 2006 and references therein). Furthermore, the mean colours of both subpopulations correlate with the mass of the host galaxy, although the relation for the blue GCs is shallower than that for the red ones (Forbes et al. 1997; Larsen et al. 2001; Peng et al. 2006).

The *red* GCs are known to share a similar 1D radial, and 2D spatial, distribution with that of the galaxy starlight in elliptical galaxies (Lee et al. 1998; Forbes et al. 2004; Dirsch et al. 2005; Lee et al. 2008; Bassino et al. 2008; Faifer et al. 2011; Strader et al. 2011). They also show similar kinematics (Norris et al. 2006, 2008; Lee et al. 2008; Pota et al. 2012) and stellar populations (Forbes & Forte 2001; Norris et al. 2006; Spitler 2010; Forbes et al. 2011) in many cases (although some exceptions do exist, e.g. Foster et al. 2011). This suggests that the red metal-rich GCs share a

common formation history with the stellar component of an elliptical galaxy.

The *blue* GCs have been associated with elliptical galaxy halos in the literature but the evidence for this is usually more indirect. Their radial surface density profiles are flatter than those of the starlight and they generally extend beyond the radius that can be accurately measured for the starlight. Forte et al. (2007, 2011) have suggested that the ‘halo’ component of elliptical galaxy starlight is associated with the blue GC subpopulation. The halos of large elliptical galaxies also contain diffuse X-ray emitting hot gas. This gas is generally thought to be in hydrostatic equilibrium, although the inner regions may experience strong cooling via bremsstrahlung and line emission, and heating from AGN (e.g. O’Sullivan et al. 2003).

In a cosmological context, rare over-dense fluctuations in the early Universe collapse first. Thus the old stellar populations in a galaxy (e.g. the halo field stars and blue metal-poor GCs) are expected to share the same spatial distribution (Moore et al. 2006) and have the same origin (Boley et al. 2009). Recent hydro-dynamical simulations have found similar power-law slopes for the *stellar* halos of Milky Way like disk galaxies (e.g.  $-2.6$  to  $-3.4$ ; Font et al. 2011) but lack the resolution to simulate GCs directly and have not yet produced realistic X-ray surface brightness profiles. In the Milky Way, both the halo field stars and the metal-poor GCs do share the same 3D spatial distribution which has

\* E-mail: dforbes@swin.edu.au

a radial power-law slope of  $\sim -3.5$  (Helmi 2008). Furthermore, it is now recognised that a significant fraction of the halo field stars come from disrupted GCs (Forbes & Bridges 2010; Martell & Grebel 2010).

As both the blue GCs and the diffuse hot gas occupy the same halo gravitational potential they may reveal the same radial distribution. Based on blue GC counts from a wide-field imaging study of Dirsch et al. (2003) and the X-ray emission detected by the ROSAT satellite, Forte et al. (2005) reported a good coincidence between the projected surface density of blue GCs and the X-ray surface brightness profile out to  $\sim 110$  kpc for the central dominant galaxy in the Fornax cluster NGC 1399. As far as we are aware this is only case in the literature of a direct comparison between the spatial distribution of blue GCs and X-ray emission. It is therefore important to understand whether NGC 1399 is a special case or whether such similarities in the projected spatial distributions are common. A hint that the latter is true comes from the work of McLaughlin (1999) who pointed out the similarity in the *total* GC system surface density profile with the combined stellar and hot gas radial profiles for M87, NGC 1399 and NGC 4472. In the halo of a galaxy, these profiles are dominated by the blue GCs and hot gas respectively.

Lee et al. (2010) studied the large-scale distribution of GC candidates through out the Virgo cluster using Sloan Digital Sky Survey data. They concluded that this distribution was qualitatively similar to that of the large-scale X-ray emission; with the blue GCs more closely resembling the X-ray emission than the red ones. Finally, we note that the global X-ray emission from giant elliptical galaxies correlates better with the velocity dispersion of the blue rather than the red GC subpopulation (Lee et al. 2008; Pota et al. 2012).

In this paper, we have collected data from the literature for a small sample of giant elliptical galaxies that have diffuse hot gas halos and radially extended GC systems that can be clearly separated into blue and red subpopulations. We explore the radial distributions of these baryonic halo tracers and briefly discuss their interpretation.

## 2 ELLIPTICAL GALAXY SAMPLE

Our sample consists of two central cluster galaxies (M87 and NGC 1399), six giant ellipticals in groups or clusters and one isolated field galaxy as listed in Table 1. Most are the central brightest galaxies in their host group/cluster (i.e. BGG/BCG). Table 1 includes the type of galaxy, its environment, hot gas temperature, distance, K-band luminosity, stellar velocity dispersion, physical scale of 1 arcmin and the source of the galaxy surface brightness profile. Apart from the field galaxy NGC 720, all are massive galaxies with  $M_K \sim -25$  ( $M_V \sim -22$ ) that dominate their group or subgroup within a cluster, i.e. lie at the centre of their local potential well and X-ray emission. In the case of the cD galaxy M87, it lies at the centre of Virgo cluster potential well whereas NGC 4472 is the brightest galaxy in the Virgo cluster dominating its own subgroup. NGC 1407 is the brightest galaxy in the massive Eridanus group (Romanowsky et al. 2009). NGC 4365 lies in the *W'* cloud, a group lying some 5 Mpc behind the Virgo cluster. NGC 4636 lies in an X-ray distinct

subgroup to the South of the main Virgo cluster. NGC 4649 is a giant Virgo elliptical galaxy. NGC 5846 is the brightest galaxy in the NGC 5846 group.

Our sample of elliptical galaxies was selected, from the literature, to have extended radial profiles for both GCs and diffuse X-ray emission. In particular, the blue GC density profile was required to extend to at least 8 arcmin (about 45 kpc at the typical distance of our sample). Further details of the selection process and literature data are discussed below.

## 3 X-RAY SURFACE BRIGHTNESS PROFILES

The X-ray emission of giant elliptical galaxies is dominated by diffuse hot gas and their surface brightness profiles tend to range from core-like to power-law in their inner regions, with an outer power-law slope. Such profiles are usually quantified by a so-called beta model, i.e.

$$S(r) = S_0[1 + (r/r_c)^2]^{-3\beta_X + 0.5} \quad (1)$$

Here we take the beta model fit parameters (i.e. the core radius  $r_c$  and the  $\beta_X$  value) from the X-ray surface brightness profiles in the literature.

Although the Chandra satellite has superior resolution and XMM-Newton has better sensitivity, the ROSAT satellite is generally preferred for its extended radial coverage when studying the outer halos of giant elliptical galaxies. For the two central cluster galaxies (M87 and NGC 1399) in our sample we use beta model fits to the ROSAT X-ray surface brightness profiles. These fits extend to over 100 arcmin for M87 (Bohringer et al. 1994) and to 40 arcmin for NGC 1399 (Jones et al. 1997). For NGC 5846 a deep (120 ksec) Chandra image is available from Machacek et al. (2011).

For the other giant ellipticals, X-ray profiles come from ROSAT data in the large sample study of O'Sullivan, Ponman & Collins (2003). A detailed description of the data reduction and analysis can be found in O'Sullivan et al. Briefly, periods of high background (deviating by  $>2\sigma$  from the mean event rate) were excluded from each dataset, point sources of  $>4.5\sigma$  significance were excluded (excepting those within the  $D_{25}$  radius of the target galaxy), and a background model determined based on a large-radius annulus. A 0.5-2 keV image was extracted and corrected for vignetting, and a flat background level was determined and subtracted from the image. A standard beta model was fit to the data, after convolution with the point spread function appropriate for the mean photon energy of the source.

All the sample galaxies, including M87 and NGC 1399, are highly X-ray luminous and gas-rich. We therefore expect individual X-ray binaries to have little, or no impact, on the surface brightness fits. In a Chandra X-ray study that included our galaxies, Diehl & Statler (2007) estimated an average unresolved fraction of  $< 8\%$ . A small number of bright point sources are visible in the O'Sullivan et al. data, and they are excluded from the fit. The remaining unresolved sources could potentially affect the fit in the galaxy core, but we are primarily interested in the outer parts of each galaxy, where GCs can be reliably detected. Here, the density of X-ray binaries will be low, and therefore very unlikely to have any significant influence on the surface brightness modelling. We also note that when X-ray binaries are

**Table 1.** Elliptical galaxy sample. Type, Environment, Distance and K-band magnitude are from NASA Extragalactic Database. X-ray temperatures are from Diehl & Statler (2008). Stellar velocity dispersions ( $\sigma_*$ ) are from HyperLeda; Surface Brightness profile. References for surface brightness (SB) profiles are: (1) Kormendy et al. (2009); (2) Goudfrooij et al. (1994); (3) Forte et al. (2005); (4) Spitler et al. (2012); (5) Blom, Spitler & Forbes (2012); (6) Caon et al. (1994); (7) MacDonald et al. (2011); (8) Kronawitter et al. (2000).

Galaxy	Type	Envir.	$T_X$ (keV)	Dist. (Mpc)	$M_K$ (mag)	$\sigma_*$ (km/s)	kpc/'	SB profile
M87	cD	Virgo	2.50	16.7	-25.29	334	4.9	(1)
NGC 720	gE	Field	0.57	24.0	-24.63	241	7.0	(2)
NGC 1399	BCG	Fornax	1.13	19.0	-25.06	346	5.5	(3)
NGC 1407	BGG	Group	0.87	23.8	-25.15	271	6.9	(4)
NGC 4365	BGG	Group	0.64	21.4	-25.00	256	6.2	(5)
NGC 4472	BCG	Virgo	0.97	16.1	-25.61	294	4.7	(6)
NGC 4636	BGG	Group	0.69	15.9	-24.57	203	4.6	(6)
NGC 4649	gE	Virgo	0.80	16.5	-25.34	335	4.8	(7)
NGC 5846	BGG	Group	0.71	26.7	-25.18	239	7.8	(8)

**Table 2.** Globular cluster data. References for surface density and filter data are: (1) Strader et al. (2011); (2) Kartha et al. (2012, in prep) (3) Bassino et al. (2006); (4) Spitler et al. (2012); (5) Blom, Spitler & Forbes (2012); (6) Rhode et al. (2011, priv. comm.); (7) Dirsch et al. (2005); (8) Lee et al. (2008); (9) Pota et al. (2012). All blue and red GC velocity dispersions are from Pota et al. (2012), except M87 from Lee et al. (2008). Total number of globular clusters are from Ashman & Zepf (1998), except for NGC 1407 from Perrett et al. (1997).

Galaxy	Density	Filters	$\sigma_{BGC}$ (km/s)	$\sigma_{RGC}$ (km/s)	$N_{GC}$
M87	(1)	gri	414	380	13000
NGC 720	(2)	gi	–	–	660
NGC 1399	(3)	CR	337	277	5410
NGC 1407	(4)	gri	239	212	2640
NGC 4365	(5)	gri	238	261	2500
NGC 4472	(6)	BVR	337	257	6300
NGC 4636	(7)	CR	236	194	3000
NGC 4649	(8)	CT <sub>1</sub>	197	218	5100
NGC 5846	(9)	gri	264	206	2200

located in GCs they are typically found in red rather than blue GCs (Paolillo et al. 2011).

We exclude all galaxies that have X-ray profiles classified as ‘uncertain’ (e.g. NGC 4552) or noted to have strong AGN activity (e.g. NGC 5128) by O’Sullivan et al. (2003).

#### 4 GLOBULAR CLUSTER SURFACE DENSITIES

The GC data used here come from a variety sources in the literature. The original imaging data should be multi-filter (to clearly distinguish the blue and red subpopulations) with a wide field-of-view (to cover a large radial range).

The first criterion of using more than one filter is met by most GC studies of giant ellipticals. Thus with sufficient numbers of GCs the system can be separated into blue and red subpopulations based on a simple colour division. Here we adopt the blue/red definitions from the original literature studies.

For the second criterion, our sample is restricted to those galaxies which have GC system surface density profiles out to at least 8 arcmin (about 45 kpc for our sample). The minimum radial extent is for NGC 4649 which reaches to 8.75 arcmin using data from Lee et al. (2008). The typical effective radius of the galaxy starlight for our sample is

5–10 kpc; thus the GC data typically probe to several effective radii in terms of the host galaxy starlight. Requiring large radial coverage of nearby galaxies effectively restricts studies to those that use a ground-based telescope. Our final sample of giant elliptical galaxies is summarised in Table 1.

All GC profiles have been corrected for background contamination in the original work. However, the level of the background contamination and the ability to subtract it accurately vary for each dataset. This uncertainty is generally not captured in the (Poisson) error bars quoted in the literature. Although good seeing conditions help for GC studies, the introduction of a third filter can significantly decrease background levels as GC candidates can be selected in colour-colour space. For example, Romanowsky et al. (2009) found a contamination rate of ~5% in follow-up spectroscopy of GCs in NGC 1407 selected from three filters. In Table 2, along with the source of the GC surface density data, we list whether it comes from 2 or 3 filter imaging. Thus the best quality GC data are available for M87, NGC 1407, NGC 4365, NGC 4472 and NGC 5846. The total number of objects in the GC system, from the literature, is also included.

Traditionally, GC surface density profiles have been fit by a simple power-law. However, this approach often fits the central regions in which the density flattens off, perhaps due to destruction effects (Miocchi et al. 2006) and hence tends

to underestimate the outer slope. A better approach, which is becoming more common (e.g. Strader et al. 2011; Blom, Spitler & Forbes 2012) is to fit Sersic (1968) profiles to the GC density data as has been done for galaxy surface brightness profiles for a number of years. Here we have decided to fit the GC surface density data with the same beta profile form as used in fits to the X-ray surface brightness data in order to facilitate a direct comparison. Such beta profiles, like Sersic ones, fit an inner core region and the changing slope of the profile.

## 5 RESULTS

### 5.1 M87

In Figure 1 we show a comparison between the GC system surface density and the X-ray emission as quantified by a beta model (Eq. 1) for the central galaxy in the Virgo cluster M87. Although not optically the brightest in the cluster, it lies at the centre of the Virgo cluster X-ray emission. In this figure, and subsequent ones, the X-ray profile has been normalised to a value of 1 at 10 arcmin radius and the GCs have been arbitrarily normalised in the vertical axis.

For the *blue* GCs we show the individual data points and a beta model fit. We also show the X-ray beta model fit and a  $\pm 5\%$  variation (a typical value for well-constrained X-ray profiles) on the  $\beta_X$  slope. The blue GCs and X-ray beta model for M87 reveal a similar slope from a few arcminutes to 30 arcminutes. Only in the inner regions, in which the X-ray emission may be affected by thermal heating associated with the AGN/jet, does the coincidence begin to break down. We note that Lee et al. (2010) measured a power-law slope of  $-1.49 \pm 0.09$  for the blue GCs within 40 arcmin, and that this compares well with our data which have a power-law slope of  $-1.54 \pm 0.04$ .

We also show the similarity between the *red* GC surface density profile and that of the galaxy starlight (from Kormendy et al. 2009). Such a connection between the red GC subpopulation and the starlight of the galaxy has been observed in many galaxies as noted in the Introduction (see Brodie & Strader 2006 for an overview).

### 5.2 NGC 1399

In Figure 2 we show the GC, X-ray and stellar profiles for the central galaxy of the Fornax cluster NGC 1399. Forte et al. (2005) highlighted the similar slopes, between 1 and 20 arcmin, of the blue GC data of Dirsch et al. (2003) and the X-ray surface brightness profile of Jones et al. (1997). Here we use the same X-ray data (rather than the more recent Chandra data of Scharf et al. (2005) which only extend to less than 2 arcmin) but show the more recent and more radially extended GC data of Bassino et al. (2006). The figure supports the claim of Forte et al. but also shows that the agreement in profile slopes begins to break down for radii beyond 20 arcmin. We note that the outer region GC data are highly sensitive to contributions from other Fornax cluster galaxies (e.g. NGC 1404; Bekki et al. 2003; Schubert et al. 2011). We also show the red GCs compared to the stellar surface brightness profile from Forte et al. (2005), again with an arbitrary normalisation. Similar to the situation in

M87, the red GCs and the starlight show consistent profile slopes.

### 5.3 NGC 5846

In Figure 3 we show the GC, X-ray and stellar profiles for the central group galaxy NGC 5846. The X-ray beta model fit, to the deep (120 ksec) Chandra X-ray surface brightness profile, is from Machacek et al. (2011). They note that the galaxy shows signs of central AGN activity (e.g. X-ray cavities) and non-hydrostatic gas motions, yet the profile is fairly well represented by a single beta model to 12 arcmin. As for M87 and NGC 1399, the red GCs are well matched to the starlight profile, while the blue GCs are consistent with the X-ray profile over most radii (the innermost regions may be affected by GC destruction processes; Miocchi et al. 2006).

### 5.4 The O’Sullivan et al. sample

In Figures 4 and 5 we show galaxies from the giant elliptical galaxy sample of O’Sullivan et al. (2003) for which we were able to find GC surface density data that extended to at least 8 arcmin (i.e. well beyond any GC core region). The figures show the *blue* GC surface density data from the literature, beta model fits to those data, and beta model fits (and their uncertainty) to the ROSAT X-ray surface brightness profiles as determined by O’Sullivan. For most galaxies the surface density of blue GCs in the outer regions is well-matched to the X-ray profile. The main exception is NGC 4365 which reveals a GC profile that is significantly flatter than the X-ray one. This galaxy is currently undergoing an interaction (Mihos et al. 2012) and it is possible that the accreted galaxy has contributed extra GCs to the outer regions ( $> 10$  arcmin) of NGC 4365.

All of the GC systems in Figures 4 and 5 reveal a flattening (i.e. towards a constant density) at small radii. This has been observed in many GC systems (Forbes et al. 1996) and may be due to GC destruction processes, such as bulge shocking (Miocchi et al. 2006).

As mentioned earlier, we have fit the blue GC surface density data with a beta model (Eq. 1). For NGC 4636 we were unable to obtain stable fits to the error-weighted data and so we chose to fit with equal weighting. The GC data for NGC 4636 show an increased density at large radii. This is likely an indication of the uncertainty in the background subtraction. If we fit only the blue GC data interior to 12.5 arcmin we derive the same beta slope within the errors quoted in Table 3. For NGC 4649 the limited radial extent did not allow for a beta model fit for the blue GCs. In this case we fit a simple power-law fit to the data beyond 4 arcmin which gives an equivalent beta slope of  $0.55 \pm 0.09$  and is quoted in Table 3. The results of our beta model fitting to the blue GC density profiles are given in Table 3, along with the  $\beta_X$  values from the X-ray surface brightness fits from the literature. Table 3 also gives mean values and the error on the mean. The X-ray and blue GC beta slopes are consistent within the errors, while the red GCs have higher beta values than the X-ray profiles at the  $\sim 2\sigma$  level.

Figures 4 and 5 also show the *red* GC data with the galaxy surface brightness profile from the literature. The

**Table 3.** Beta slope values for X-ray and globular cluster radial profiles. References for X-ray data are: (1) Bohringer et al. (1994); (2) O’Sullivan et al. (2003); (3) Jones et al. (1997); (4) Machacek et al. (2011).

Galaxy	X-ray	$\beta_X$	$\beta_{BGC}$	$\beta_{RGC}$
M87	(1)	0.47	$0.43 \pm 0.13$	$0.49 \pm 0.01$
NGC 720	(2)	$0.483 \pm 0.01$	$0.60 \pm 0.09$	$0.72 \pm 0.12$
NGC 1399	(3)	0.35	$0.42 \pm 0.05$	$0.51 \pm 0.02$
NGC 1407	(2)	$0.56^{+0.02}_{-0.01}$	$0.58 \pm 0.17$	$0.86 \pm 0.04$
NGC 4365	(2)	$0.60^{+0.04}_{-0.03}$	$0.46 \pm 0.12$	$0.61 \pm 0.03$
NGC 4472	(2)	$0.597^{+0.009}_{-0.008}$	$0.67 \pm 0.22$	$0.52 \pm 0.02$
NGC 4636	(2)	$0.535^{+0.007}_{-0.006}$	$0.69 \pm 0.09$	$0.53 \pm 0.02$
NGC 4649	(2)	$0.567 \pm 0.08$	$0.55 \pm 0.09$	$0.63 \pm 0.11$
NGC 5846	(4)	0.45	$0.51 \pm 0.10$	$0.54 \pm 0.09$
Mean	–	$0.51 \pm 0.03$	$0.54 \pm 0.03$	$0.60 \pm 0.04$

galaxy profiles are from Goudfrooij et al. (1994) for NGC 720; Spitler et al. (2012) for NGC 1407; Blom, Spitler & Forbes (2012) for NGC 4365; Caon et al. (1994) for NGC 4472 and NGC 4636 and MacDonald et al. (2011) for NGC 4649. Although the galaxy starlight does not extend as far as the GC data (particularly for NGC 720), the GCs and the starlight show similar slopes in their outer regions. Given that the blue and red GCs occupy the same gravitational potential but have different density profiles, the Jeans equation suggests that they also have different orbital anisotropy properties.

## 5.5 Summary

We support previous findings that the *red* GC density profiles generally follow the starlight in elliptical galaxies. Most elliptical galaxies in the sample show good coincidence between the outer slope of the *blue* GC profile and the X-ray surface brightness. We note that the measured GC slopes are dependent on the level of background contamination and hence the overall quality of the data which is not captured by the purely Poisson errors given in the literature. The average slopes of the blue GCs and X-ray emission are consistent within the errors, although our sample is small.

## 6 DISCUSSION

In the previous section we showed that the outer slope of the X-ray emission (with a mean slope of  $\beta_X = 0.51 \pm 0.03$ ) was in good agreement, in most cases, with the blue GCs surface density slope (mean  $\beta_{BGC} = 0.54 \pm 0.03$ ). Could this similarity between the projected blue GC and X-ray profiles indicate a direct physical connection between the metal-poor GC system and the diffuse hot gas in an elliptical galaxy halo? One possibility is that GCs have formed within hot gas that permeates the halos of giant ellipticals. For example, in the model of Fall & Rees (1985) the hot gas acts to compress colder gas clouds. For metal-poor gas this gives rise to a characteristic mass of  $\sim 10^6 M_\odot$  which is typical of GCs. However a problem with this scenario is that metal-poor GCs also form in dwarf galaxies which lack hot gas halos.

More probably, the coincidence in profile shape between blue GCs and X-ray emission from hot gas reflects the fact

that for our giant elliptical galaxy sample both halo tracers are in equilibrium within the potential well centred on the host galaxy. The observed correlations of hot gas X-ray emission and the blue GC velocity dispersion (Lee et al. 2008; Pota et al. 2012) further supports this interpretation.

If this is the case, then the similar outer slopes seen for the blue GCs and the X-ray emission has an interesting implication for the relative density profiles of the two tracers and their specific energies. The X-ray emissivity, which projects to give surface brightness, is proportional to the square of the hot gas density, whereas the projected GC surface density scales linearly with the GC density. So similar outer slopes in projection imply that the hot gas density scales with the GC density to the power of 0.5. In other words, the GCs have a steeper 3D radial density distribution than the hot gas.

The radial distribution of a tracer in equilibrium within a gravitational potential well is related to its specific energy, and hence the relative slopes of the gas and GC profiles will depend on the ratios of their specific energies, traditionally denoted  $\beta_{spec}$  in the cluster literature. In our case:

$$\beta_{spec} = 0.5(3\sigma_{BGC}^2) / (3kT_X/2m), \quad (2)$$

where  $\sigma_{BGC}$  is the blue GC velocity dispersion,  $T_X$  is the hot gas temperature,  $k$  is the Boltzman constant and  $m$  is the mean particle mass of the hot gas. Using  $m = 0.6$  amu, this reduces to:

$$\beta_{spec} = (\sigma_{BGC} / 1000 \text{ km s}^{-1})^2 (6.22 \text{ keV}/T_X). \quad (3)$$

Taking X-ray temperatures ( $T_X$ ) from Table 1 and blue velocity dispersions ( $\sigma_{BGC}$ ) from Table 2, the resulting  $\beta_{spec}$  values have a mean of 0.52 for our sample. In other words, the blue GCs have about half the specific energy of the hot gas.

Assuming that the GCs are virialised and follow the Jeans equation, and the hot gas is in hydrostatic equilibrium, the value of  $\beta_{spec}$  is related to the gradients in the density and temperature/velocity dispersion of the two tracers by equation 35 from Bahcall & Lubin (1994).

Although kinematic studies of GCs are limited, to first order blue GCs reveal flat velocity dispersion profiles (e.g. Lee et al. 2008; Pota et al. 2012). The orbital anisotropy for blue GCs is not well determined but orbits appear to be

close to isotropic on average. Similarly, X-ray temperature profiles, beyond the very inner regions, are close to flat on average (O’Sullivan et al. 2003). For the case of isotropic GC orbits with flat velocity dispersion gradient and isothermal gas, the equation simplifies such that:

$$\beta_{spec} = \frac{d \ln \rho_{gas} / d \ln r}{d \ln \rho_{BGC} / d \ln r} \quad (4)$$

where  $\rho_{gas}$  and  $\rho_{BGC}$  are the density of hot gas and blue GCs respectively.

Hence, since we find  $\beta_{spec} \sim 0.5$ , it follows that we would expect the logarithmic slope of the gas density to be one half of that of the blue GCs, and hence the X-ray emissivity (scaling as density squared) would indeed have the same slope as the density of blue GCs.

For a beta model (Eq. 1) the logarithmic slope at large radii is given by  $-6\beta + 1$ . Given the mean beta value for the blue GCs of  $\beta_{BGC} = 0.54$  this corresponds to a projected outer slope of -2.24. If the GCs have spherical symmetry then the *deprojected* 3D slope for the blue GCs will be -3.24 (in comparison the surface density of blue GCs in the Milky Way has a 3D slope of -3.5; Helmi 2008). In comparison, the projected X-ray emissivity (with mean  $\beta_X = 0.51$  from Table 3) has a slope of -2.06, and hence a 3D slope of -3.06, so that the average 3D gas density slope is -1.53, roughly one half that of the blue GCs.

This result is reminiscent of that found by Osmond & Ponman (2004) for galaxy groups. They derived the specific energy of the galaxies and compared it to that for the hot gas in galaxy groups. The groups had a mean  $\beta_{spec} = 0.75$  indicating that the galaxies had a lower specific energy than the hot gas within the group. (We note that galaxy clusters have  $\beta_{spec} \sim 1$ .) Here, we find that the blue GCs have a specific energy ( $\beta_{spec} \sim 0.5$ ) lower than that of galaxies in groups and much lower than the expected value for the group potential. Thus whatever process gives rise to blue GCs in the halos of giant elliptical galaxies must deposit them with a relatively low specific energy. If blue GCs have been accreted relatively recently then the likely source would be more massive galaxies which, unlike dwarfs, are able to lose specific energy on a Gyr timescale through dynamical friction. However, perhaps more likely is the accretion and disruption of dwarf galaxies at early times when the group/cluster was less massive than today.

## 7 SUMMARY AND CONCLUSIONS

For our sample of 9 giant ellipticals we have shown that the 1D radial surface density of *red* GCs, beyond the inner regions, is well matched to the stellar surface brightness profile. Thus, combining with literature studies, *red* GCs have the following properties:

- similar 1D radial distribution to the host galaxy stars
- similar 2D spatial distribution to the host galaxy stars
- similar stellar populations to the host galaxy stars
- correlate with galaxy stellar mass and stellar velocity dispersion

The *blue* GCs in the Milky Way share many properties with the stellar halo. For elliptical galaxies the connection between the *blue* GCs and the hot gas halo was based

on the similarity in 1D radial profiles for one galaxy, NGC 1399 (Forte et al. 2005). Here we have revisited NGC 1399 and included an additional 8 giant ellipticals, finding that in most cases there is a good coincidence between the outer slopes of the *blue* GC surface density and the X-ray surface brightness. Thus we provide evidence for a connection between *blue* GCs and the halos of elliptical galaxies that until now was largely conjecture. This finding means we can use *blue* GCs as a halo tracer for lower luminosity ellipticals for which the X-ray emission is undetected.

As the X-ray emission scales with gas density squared and blue GC surface density scales linearly with GC density, the similarity in *projected* outer slopes implies that the 3D density distribution of the hot gas scales with the blue GC density to the power of a half. Consistent with this, we calculate that the specific energy of the blue GCs is about one half that of the hot gas.

## ACKNOWLEDGMENTS

We would like to thank A. Romanowsky, R. Crain, J. Strader, C. Frenk and G. Poole for useful discussions. Thanks to V. Pota, K. Woodley, K. Rhode, L. Spitler and S. Kartha for supplying globular cluster profile data. EOS acknowledges support from the European Community under the Marie Curie Research Training Network, and from the National Aeronautics and Space Administration through Chandra Award Number AR1-12014X issued by the Chandra X-ray Observatory Center, which is operated by the Smithsonian Astrophysical Observatory for and on behalf of the National Aeronautics and Space Administration under contract NAS8-03060. Some data used in this research comes from the Hyperlede and NED databases. We also thank the referee for their careful reading and useful comments.

## REFERENCES

- Ashman, K., Zepf, S., 1998, *Globular Cluster Systems*, Cambridge University Press.
- Auger M. W., Treu T., Gavazzi R., Bolton A. S., Koopmans L. V. E., Marshall P. J., 2010, *ApJ*, 721, L163
- Bahcall N. A., Lubin L. M., 1994, *ApJ*, 426, 513
- Bassino L. P., Faifer F. R., Forte J. C., Dirsch B., Richtler T., Geisler D., Schuberth Y., 2006, *A&A*, 451, 789
- Bassino L. P., Richtler T., Dirsch B., 2008, *MNRAS*, 386, 1145
- Bekki, K., Forbes, D., Beasley, M., Couch, W., 2003, *MNRAS*, 344, 1334
- Blom C., Spitler L. R., Forbes D. A., 2012, *MNRAS*, 420, 37
- Blom, C., et al. 2012, in prep.
- Böhringer H., Briel U. G., Schwarz R. A., Voges W., Hartner G., Trümper J., 1994, *Natur*, 368, 828
- Boley A. C., Lake G., Read J., Teyssier R., 2009, *ApJ*, 706, L192
- Brodie J. P., Strader J., 2006, *ARA&A*, 44, 193
- Caon N., Capaccioli M., D’Onofrio M., 1994, *A&AS*, 106, 199
- Crain R. A., McCarthy I. G., Frenk C. S., Theuns T., Schaye J., 2010, *MNRAS*, 407, 1403

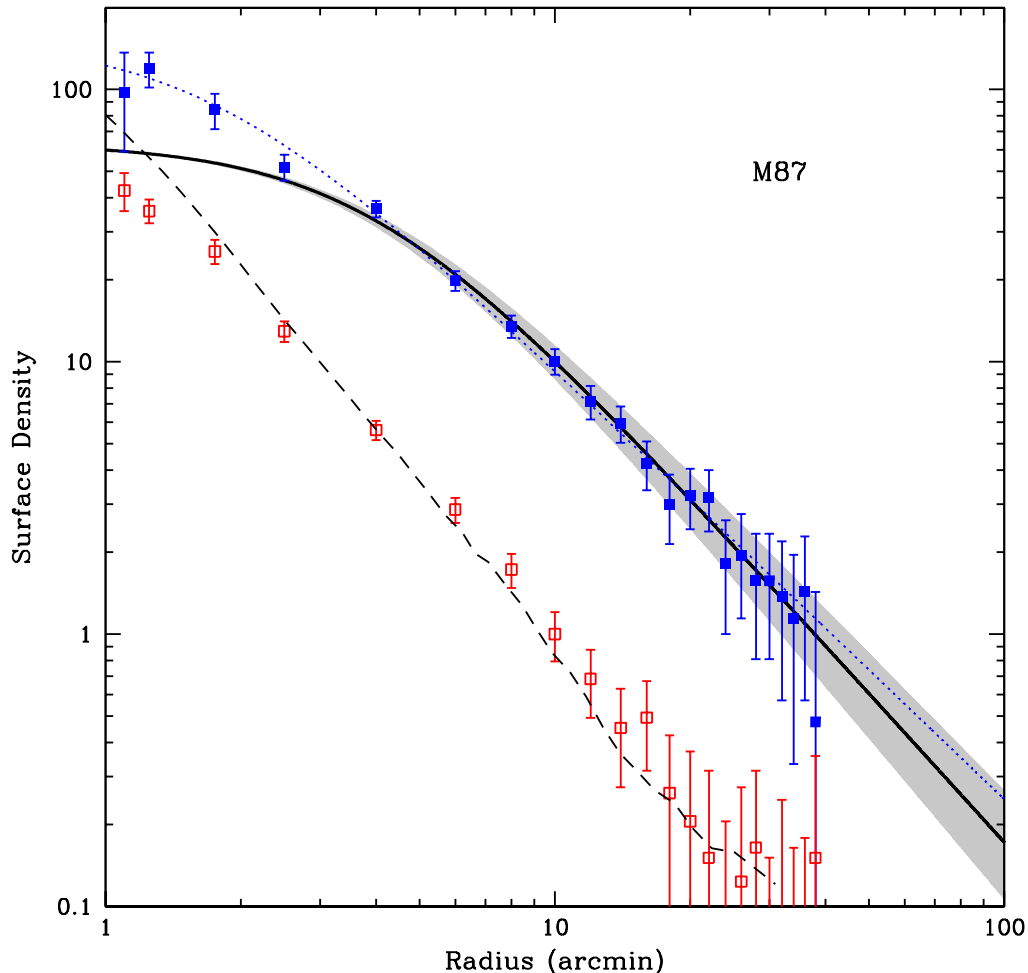


**Figure 1.** Globular cluster and X-ray surface density profiles for the central dominant Virgo galaxy M87. The blue (blue filled squares) and red (red open squares) globular cluster system density profiles are shown along with a beta model fit to the blue GC data (dotted line). The X-ray surface brightness from a beta model fit to beyond 100 arcmin (solid line) with a  $\pm 5\%$  slope uncertainty (shaded region) and the galaxy starlight profile from Kormendy et al. (2009) (dashed line) are also shown. All profiles have an arbitrary vertical normalisation. The red GCs follow the galaxy stellar component while the blue GCs trace the X-ray profile.

Diehl S., Statler T. S., 2007, *ApJ*, 668, 150  
 Diehl S., Statler T. S., 2008, *ApJ*, 687, 986  
 Dirsch B., Richtler T., Geisler D., Forte J. C., Bassino L. P., Gieren W. P., 2003, *AJ*, 125, 1908  
 Dirsch B., Schubert Y., Richtler T., 2005, *A&A*, 433, 43  
 Drinkwater M. J., Gregg M. D., Colless M., 2001, *ApJ*, 548, L139  
 Faifer F. R., et al., 2011, *MNRAS*, 416, 155  
 Fall S. M., Rees M. J., 1985, *ApJ*, 298, 18  
 Forbes D. A., Franx M., Illingworth G. D., Carollo C. M., 1996, *ApJ*, 467, 126  
 Forbes D. A., Brodie J. P., Grillmair C. J., 1997, *AJ*, 113, 1652  
 Forbes D. A., Brodie J. P., Larsen S. S., 2001, *ApJ*, 556, L83  
 Forbes D. A., Forte J. C., 2001, *MNRAS*, 322, 257  
 Forbes D. A., et al., 2004, *MNRAS*, 355, 608  
 Forbes D. A., Bridges T., 2010, *MNRAS*, 404, 1203

Forbes D. A., Spitler L. R., Strader J., Romanowsky A. J., Brodie J. P., Foster C., 2011, *MNRAS*, 413, 2943  
 Forte J. C., Faifer F., Geisler D., 2005, *MNRAS*, 357, 56  
 Forte J. C., Faifer F., Geisler D., 2007, *MNRAS*, 382, 1947  
 Forte J. C., Vega, E. I., Faifer F., 2011, *MNRAS*, in press  
 Font A. S., McCarthy I. G., Crain R. A., Theuns T., Schaye J., Wiersma R. P. C., Dalla Vecchia C., 2011, *MNRAS*, 1162  
 Ghizzardi S., Molendi S., Pizzolato F., De Grandi S., 2004, *ApJ*, 609, 638  
 Goudfrooij P., Hansen L., Jorgensen H. E., Norgaard-Nielsen H. U., de Jong T., van den Hoek L. B., 1994, *A&AS*, 104, 179  
 Helmi A., 2008, *A&ARv*, 15, 145  
 Jones C., Stern C., Forman W., Breen J., David L., Tucker W., Franx M., 1997, *ApJ*, 482, 143  
 Koopmans L. V. E., et al., 2009, *ApJ*, 703, L51

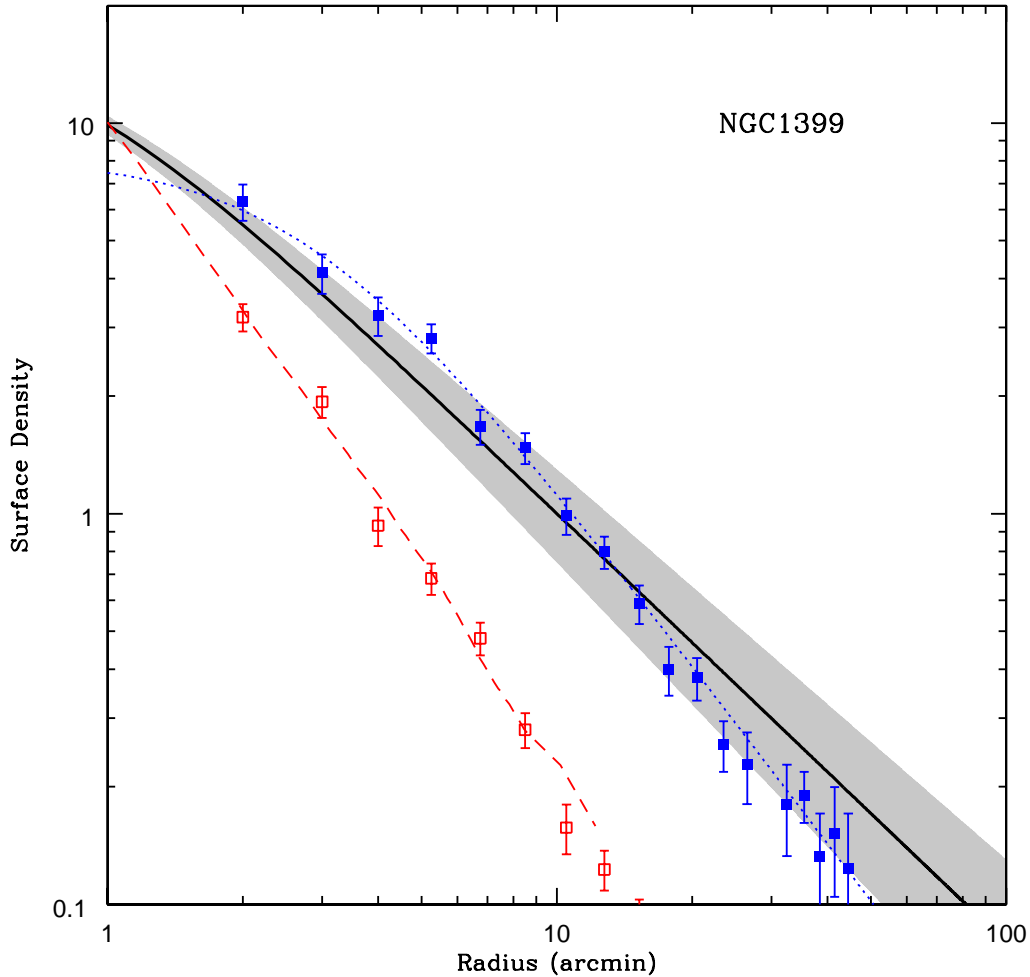


**Figure 2.** Globular cluster and X-ray surface density profiles for the central dominant Fornax galaxy NGC 1399. The blue (blue filled squares) globular cluster density profile is shown along with a beta model fit to the blue GC data (dotted line). The X-ray surface brightness from a beta model fit to radii  $\leq 40$  arcmin (solid line) with a  $\pm 5\%$  slope uncertainty (shaded region) is shown. We also show the red (red filled squares) globular cluster density profile along with the galaxy starlight profile from Forte et al. (2005) (long dashed line). All profiles have an arbitrary vertical normalisation. The red GCs follow the galaxy stellar component while the blue GCs have a similar slope to the X-ray profile.

Kormendy J., Fisher D. B., Cornell M. E., Bender R., 2009, *ApJS*, 182, 216  
 Larsen S., Brodie J. P., Huchra J. P., Forbes D. A., Grillmair C. J., 2001, *AJ*, 121, 2974  
 Lee M. G., Kim E., Geisler D., 1998, *AJ*, 115, 947  
 Lee M. G., Park H. S., Kim E., Hwang H. S., Kim S. C., Geisler D., 2008, *ApJ*, 682, 135  
 Lee M. G., Park H. S., Hwang H. S., 2010, *Sci*, 328, 334  
 McDonald M., Courteau S., Tully R. B., Roediger J., 2011, *MNRAS*, 414, 2055  
 Machacek, M., et al. 2011, *ApJ*, 743, 15  
 Martell S. L., Grebel E. K., 2010, *A&A*, 519, A14  
 McLaughlin D. E., 1999, *AJ*, 117, 2398  
 Mei S., et al., 2007, *ApJ*, 655, 144  
 Mihos, C., et al. 2012, in prep.  
 Miocchi P., Capuzzo Dolcetta R., Di Matteo P., Vicari A., 2006, *ApJ*, 644, 940

Moore B., Diemand J., Madau P., Zemp M., Stadel J., 2006, *MNRAS*, 368, 563  
 Norris M. A., Sharples R. M., Kuntschner H., 2006, *MNRAS*, 367, 815  
 Norris M. A., et al., 2008, *MNRAS*, 385, 40  
 Osmond J. P. F., Ponman T. J., 2004, *MNRAS*, 350, 1511  
 O’Sullivan E., Ponman T. J., Collins R. S., 2003, *MNRAS*, 340, 1375  
 Paolillo M., Puzia T. H., Goudfrooij P., Zepf S. E., Maccarone T. J., Kundu A., Fabbiano G., Angelini L., 2011, *ApJ*, 736, 90  
 Pellegrini S., Ciotti L., 1998, *A&A*, 333, 433  
 Peng E. W., et al., 2006, *ApJ*, 639, 95  
 Perrett K. M., Hanes D. A., Butterworth S. T., Kavelaars J., Geisler D., Harris W. E., 1997, *AJ*, 113, 895  
 Pota, V., et al. 2012, in prep.

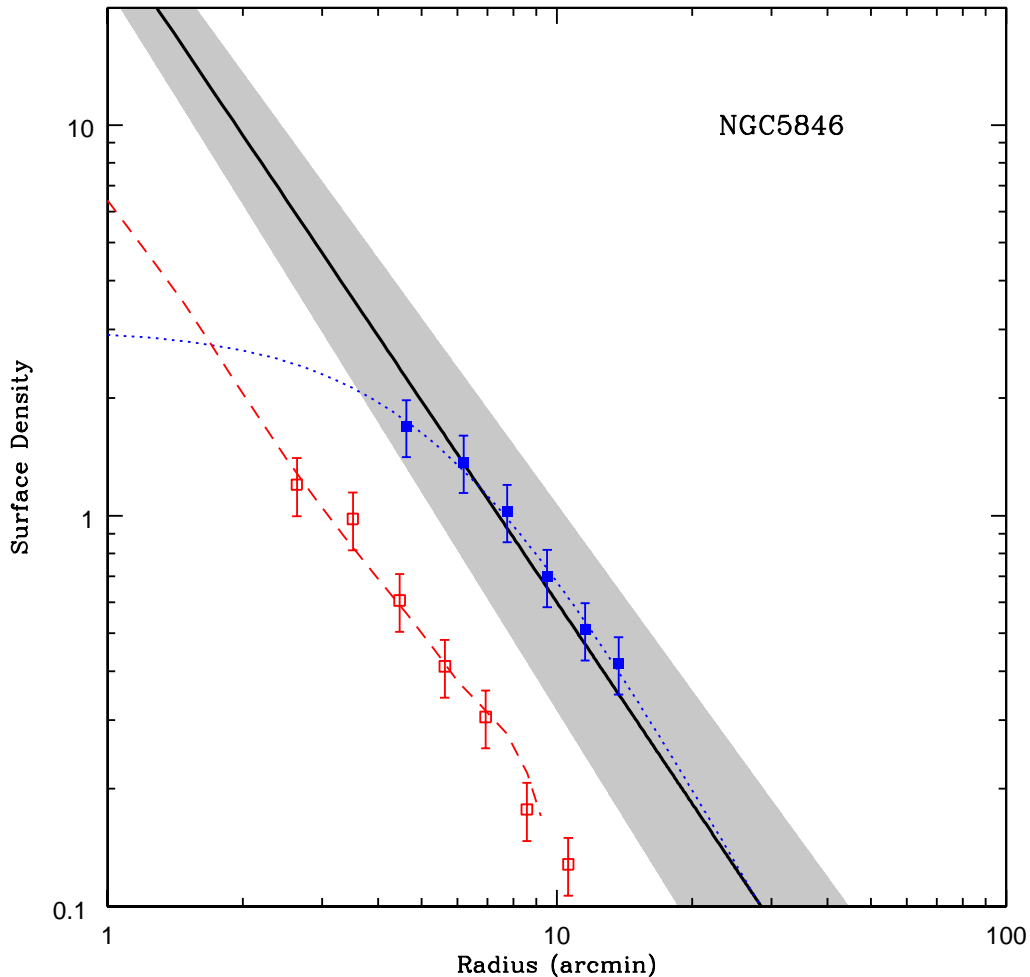


**Figure 3.** Globular cluster and X-ray surface density profiles for the central group galaxy NGC 5846. The blue (blue filled squares) globular cluster density profile is shown along with a beta model fit to the blue GC data (dotted line). The X-ray surface brightness from a beta model fit to radii  $\leq 12$  arcmin (solid line) with a  $\pm 5\%$  slope uncertainty (shaded region) is shown. We also show the red (red filled squares) globular cluster density profile along with the galaxy starlight profile from Kronawitter et al. (2000) (long dashed line). All profiles have an arbitrary vertical normalisation. The red GCs follow the galaxy stellar component while the blue GCs have a similar slope to the X-ray profile.

Romanowsky A. J., Strader J., Spitler L. R., Johnson R.,  
 Brodie J. P., Forbes D. A., Ponman T., 2009, *AJ*, 137,  
 4956  
 Scharf, C., Zurek, D., Bureau, M., 2005, *ApJ*, 633, 154  
 Schubert, Y., Richtler, T., Hilker, M., Dirsch, B.,  
 Bassino, L., Romanowsky, A., Infante, L., *A&A*, 513, 52  
 Sersic J. L., 1968, *Atlas de Galaxias Australes*, Observa-  
 torio Astronomico, Cordoba, Argentina  
 Spitler L. R., 2010, *MNRAS*, 406, 1125  
 Spitler L. R., et al. 2012, *MNRAS*, in press  
 Strader J., et al. 2011, *ApJS*, in press  
 Woodley K. A., Gómez M., Harris W. E., Geisler D.,  
 Harris G. L. H., 2010, *AJ*, 139, 1871

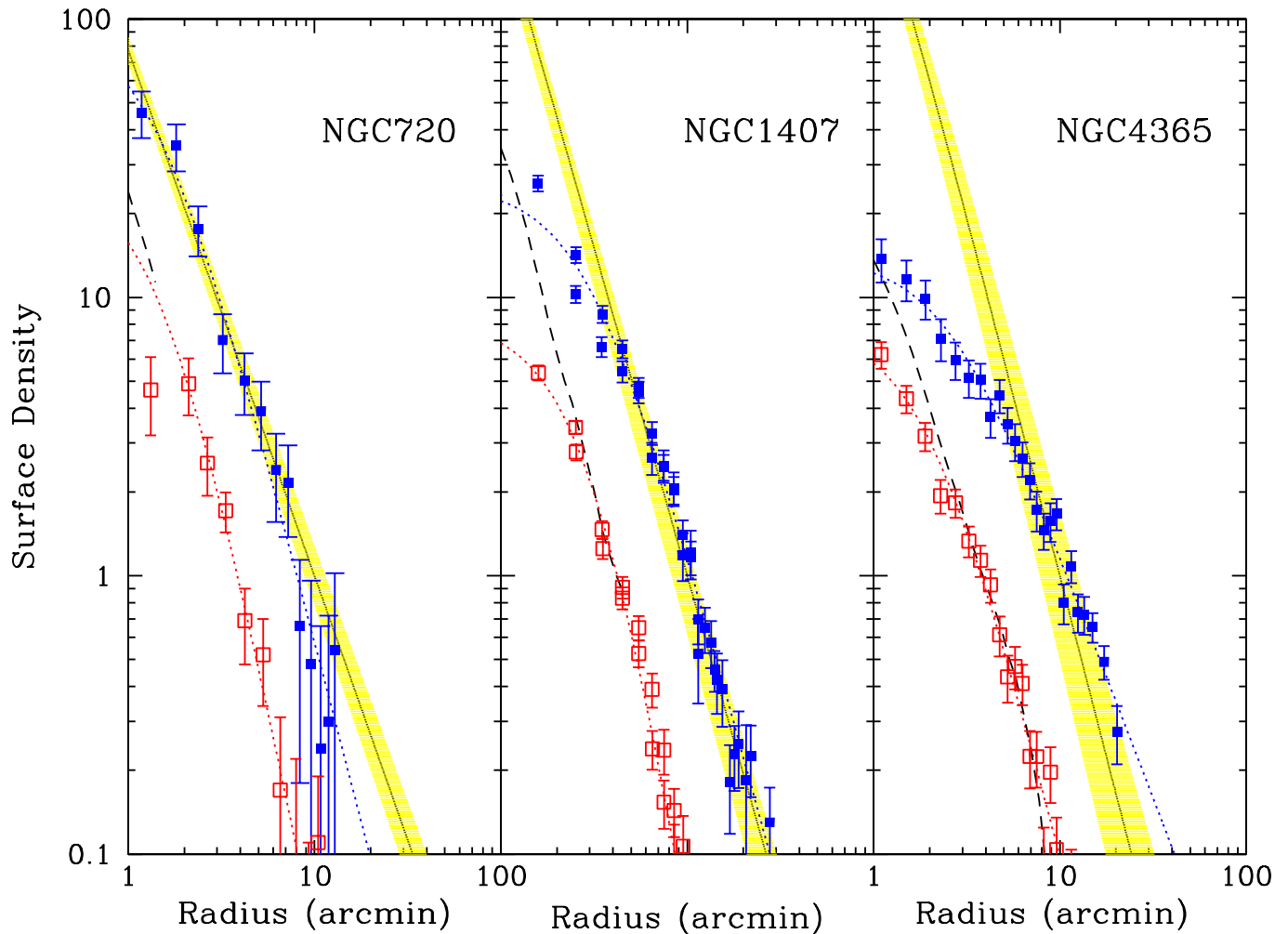


**Figure 4.** Globular cluster and extrapolated X-ray surface density profiles for NGC 720, 1407 and 4365. The X-ray surface brightness beta model fits and uncertainty (line and yellow shaded region) are all taken from the survey of O’Sullivan et al. (2003). The blue (blue filled squares) and red (red open squares) globular cluster density profiles are shown along with a beta model fits (blue and red dotted lines). The galaxy surface brightness profile is shown by a white dashed line. All profiles have an arbitrary vertical normalisation. For most galaxies, the outer slopes of the X-ray and blue GC profiles are similar, as are the galaxy surface brightness and red GC profiles.

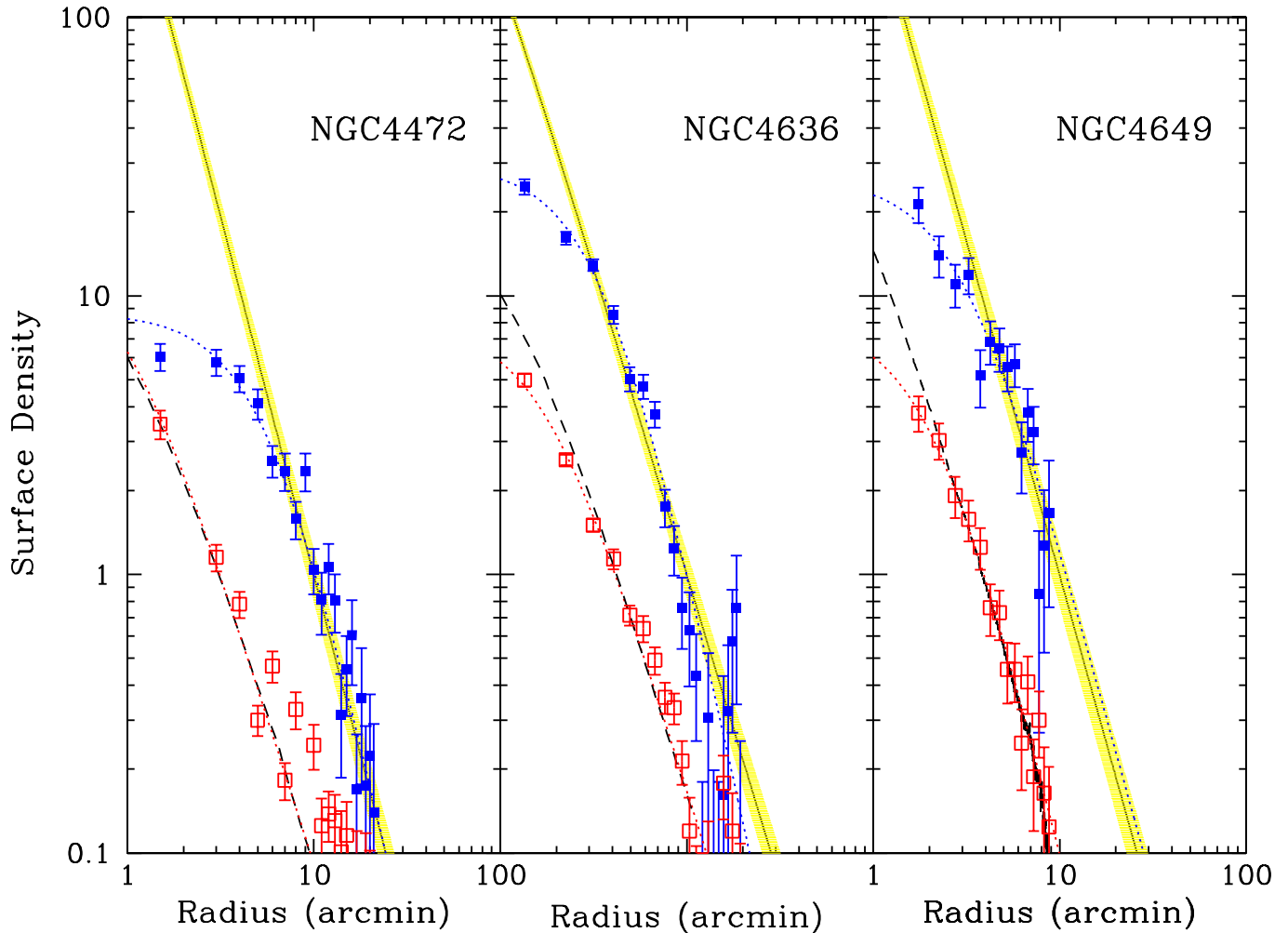


**Figure 5.** Globular cluster and extrapolated X-ray surface density profiles for NGC 4472, 4636 and 4649. The X-ray surface brightness beta model fits and uncertainty (line and yellow shaded region) are all taken from the survey of O’Sullivan et al. (2003). The blue (blue filled squares) and red (red open squares) globular cluster density profiles are shown along with a beta model fits (blue and red dotted lines). The galaxy surface brightness profile is shown by a dashed line. All profiles have an arbitrary vertical normalisation. For most galaxies, the outer slopes of the X-ray and blue GC profiles are similar, as are the galaxy surface brightness and red GC profiles.